Journal Pre-proof

Minimal requirements for the vibration-based identification of the axial force, the bending stiffness and the flexural boundary conditions in cables

M. Geuzaine, F. Foti, V. Denoël

PII: S0022-460X(21)00384-9
DOI: https://doi.org/10.1016/j.jsv.2021.116326
Reference: YJSVI 116326

To appear in: *Journal of Sound and Vibration*

Received date : 5 November 2020
Revised date : 15 June 2021
Accepted date : 27 June 2021

Minimal requirements for the vibration-based identification of the axial force, the bending stiffness and the flexural boundary conditions in cables

M. Geuzaine[a,c], F. Foti[b], V. Denoël[a]

[a] *Structural & Stochastic Dynamics, Structural Engineering Division, University of Liège, Liège, Belgium*
[b] *Department of Civil and Environmental Engineering, Politecnico di Milano, Milano, Italy*
[c] *F.R.S.-FNRS, National Fund for Scientific Research, Brussels, Belgium*

Abstract

This paper aims at presenting the guidelines to follow in order to set up an identification procedure which is able to determine the axial force, the flexural rigidity and the rotational end stiffnesses of slender and tensioned structural elements, based on measurements of their natural frequencies and mode shapes. First of all, when such an element is slightly affected by bending stiffness effects, perturbation methods can be applied to get a composite approximation for its natural frequencies and an asymptotic expression for its mode shapes. These simple analytical formulas allow to understand the role played by each model parameter in the modal response and show that the axial force, the flexural rigidity and the rotational end stiffnesses can be correctly identified under some conditions, which are established and provided in this document. Among others, it is necessary that the identification procedure relies on the first few natural frequencies and mode shapes, which are measured near each extremity of the element, as well as some natural frequencies associated with higher modes.

Keywords: structural health monitoring, cable tension, end restraints, flexural rigidity, identification, mode shape, natural frequency

Nomenclature

Capital letters (*e.g.* L, EI, T, K_0, K_1) refer to the model parameters. The developments presented in this paper are based on a characteristic lengthscale x_r and a characteristic timescale t_r. These quantities are used to define dimensionless ones which are all referred to with greek symbols. The space coordinate x and the time t are the two independent variables of the problem; the corresponding dimensionless quantities are denoted ξ and τ. The other greek symbols refer to the problem parameters, e.g. ε^2 is the dimensionless bending stiffness.

Bold lowercase symbols (e.g. $\mathbf{r}$, $\mathbf{s}$) refer to vectors; bold capital symbols (e.g. $\mathbf{B}$) are used for matrices. In the paper, five major sets of frequencies are considered: ω_n corresponds to numerical values (which serve as a reference), ω_t and ω_b are the frequencies obtained with the taut-string model and the beam model respectively, while ω_ρ and ω_f are obtained with an asymptotic approach. A generic version is noted $\omega_\#$ where $\#$ is any of the symbols in the set $\{n, t, b, \rho, f\}$.

Email address: mgeuzaine@uliege.be, francesco.foti@polimi.it, v.denoel@uliege.be (V. Denoël)

1. Introduction

Cables in cable-stayed bridges, hangers in tied-arch bridges, external tendons in box girder bridges, diagonal braces in buildings and ties in tensegrity modules provide a few examples of key structural elements resisting high tensile stresses to ensure the overall stability of crucial structures. The regular determination of the actual tension levels inside these elements is therefore essential to monitor the health state of the structure throughout its lifetime and to detect potential harmful damages from the associated redistribution of forces, at earlier stages than those revealed by visual inspections [1, 2].

Highly tensioned members are also most often slender, lightweight, slightly damped and thus particularly susceptible to wind, human or traffic induced vibrations [3, 4]. Stress variations are consequently concentrating in the anchorages zones which are, hence, exposed to structural fatigue [5, 6] in addition to corrosion due to environmental loadings, such as rain or humidity [7, 8]. The supports are therefore critical parts of the structure, most of the damages are suspected to locate over them, but they are known to be difficult to examine visually [9, 7]. By tracking the evolution of their structural properties in time, for instance their rotational rigidity, it could be easier to regularly check their condition and to determine the positions of most of the damaged areas without requiring advanced numerical methods [10, 11].

Given the difficulty, not to say the impossibility, to install hydraulic jacks or load cells on existing structures and to calibrate elasto-magnetic sensors or strain gauges on site [12, 13], it is more convenient and affordable to use a nondestructive dynamic testing technique to identify indirectly the structural properties of an element from its natural frequencies and possibly the associated mode shapes which are typically extracted from transverse vibration signals recorded by easy-to-operate accelerometers [14, 15] or which are, more recently, coming from the processing of video images taken by multiple digital recording devices [16, 17]. The only limitation of this approach lies in the necessary mathematical model which has to interlink the structural properties of a given element with its modal characteristics, since the reliability of the identification procedure and the identifiability of the target parameters will inherently depend on the predictive capabilities of this underlying structural model and on its sensitivity to each parameter.

At the beginning, vibration-based methods were principally employed to estimate the axial force inside flexible and extensible elements by assimilating them to taut strings, whose tension can be related to the measured natural frequencies through a simple analytical formula, involving solely the prior knowledge of the length and the mass per unit length of the element [18, 19]. While the sagging effects can always be discarded, even for elements with a low extensibility, a small tension-to-weight or a large sag-to-span ratio, provided their transverse vibrations are measured horizontally [20, 3], the bending stiffness effects have to be taken into account for shorter, less loaded or flexurally more rigid elements in order to get a correct estimate of their internal tensile force [21, 22]. It consequently provides the opportunity to treat their flexural rigidity as an additional unknown in the identification procedure [23, 24], since it affects the natural frequencies and the mode shapes of the element but is difficult to determine in advance due to complex internal geometries or to poor information about the materials. Moreover, non-negligible bending stiffness effects interestingly reveal the influence of the rotational end restraints on the dynamics of the cable.

Over the years, empirical and practical formulas [24, 25] have been developed to take these effects into account. Whereas they are mostly dedicated to cables with either perfectly hinged [26], either perfectly clamped boundary conditions [27], in practice, the end restraints are rarely infinitely flexible or infinitely rigid in rotation and are rather comprised between these two extreme cases [21]. Similarly to the flexural rigidity of the element, the proper definition of the rotational stiffnesses of its end restraints is challenging because it depends on structural details, on the specific technology adopted to fix the element at its extremities, on geometric imperfections but also on time-dependent variables, such as the aging of the support devices or the potential evolution of their degradation. These structural parameters can therefore be added to the list of unknowns to identify as well.

On the sole basis of measured natural frequencies, which are not modified by the swapping of the two rotational end restraints, existing methods have shown that it is only possible to determine a single dimensionless group, accounting for both of them all at once [28], when the measurements are corrupted by external noise or when the model contains epistemic uncertainties. However, by complementing the natural frequencies with synchronous measurements of the dynamic deflections of the element at several locations along its length, its rotational end restraints [29] can be identified after its axial force [30] when its bending stiffness is known in advance, by contrast with the recent attempts to make the simultaneous identification of both the axial force and the bending stiffness regardless of the boundary conditions [31, 17, 32].

In the present paper, we formulate necessary conditions that need to be fulfilled for an identification procedure to be effective. A mathematical model is employed to explain the reasons why some existing methods fail or struggle at identifying all together the axial force, the flexural rigidity and the rotational stiffnesses, when the considered element has a small bending stiffness. To do so, in Section 2, we first derive simple analytical formulas for the composite approximations of the natural frequencies and of the mode shapes which take into account this whole set of parameters. The asymptotic expressions are subsequently used to determine how each structural parameter influences the modal response of slender and highly tensioned members. It is ultimately possible to define some guidelines gathering the necessary conditions to set up an appropriate identification procedure. These minimal requirements are finally presented and challenged by means of numerical simulations or references from the literature in Section 3.

2. Modal analysis of a cable with arbitrary rotational end restraints

2.1. Governing equations

Figure 1 illustrates the structural model employed in this paper to represent a cable of length L, with constant bending stiffness EI, axial stiffness EA and mass per unit length M, subjected to a tensile force $T > 0$. Provided this structural element is sufficiently slender, extensible ($EA \gg T$) and tensioned ($T \gg MLg$) to neglect the sagging [20], the shear deformability and the rotational inertia effects [33], its free transverse vibrations $v\,(x, t)$ about its static equilibrium configuration are governed by the partial differential equation

$$EI\ \partial_x^4 v - T\ \partial_x^2 v + M\ \partial_t^2 v = 0 \tag{1}$$

where $t \in \mathbb{R}^+$ is the time and $x \in [0, L]$ is the position on the cable chord [3]. The equation of motion is then assorted with the four boundary conditions

$$\begin{cases} v\,(0,t) = 0 \\ v\,(L,t) = 0 \\ EI\partial_x^2 v\,(0,t) - K_0 \partial_x v\,(0,t) = 0 \\ EI\partial_x^2 v\,(L,t) + K_1 \partial_x v\,(L,t) = 0 \end{cases} \tag{2}$$

which translate the fixity in translation and the rotational equilibrium of both ends of the cable. As it is schematically depicted in Figure 1, the supports of the cable are supposed to be flexible in rotation and are accordingly modeled by rotational springs, whose stiffnesses are $K_i \geq 0$, with the subscript $i = 0$ for the left end and the subscript $i = 1$ for the right one.

Cables are commonly connected to structural components with markedly different dynamic properties (mass, stiffness, damping), such as in the paradigmatic case of stay cables linking the deck and towers of cable-stayed bridges. Strong differences between the dynamic properties of the interconnected structural elements or substructures often lead to modal localization phenomena, hinting a "quasi-independent" dynamic behavior [34, 35] and naturally leading to a clear distinction between global modes of the overall structure and local modes of the cables [36, 37, 38, 35]. Dynamic interaction and local-global mode hybridization phenomena can always occur and are typically associated to internal resonance conditions between a pair of local-global modes of the structure. Although potentially relevant for the study of the overall dynamic response of the structure, these interaction phenomena typically do not affect a significant number of the lower local modes of a cable, as it has been clearly highlighted through both analytical and experimental investigations on cable-deck and cable-tower dynamic coupling in cable-stayed bridges [18, 35, 39, 37].

Based on the above remarks, cable axial force identification procedures usually rely on analytical models describing the local dynamics of stay cables. Within this context, the dynamic coupling between the cable and the surrounding substructures is generally neglected and boundary conditions are defined in the form of either perfectly

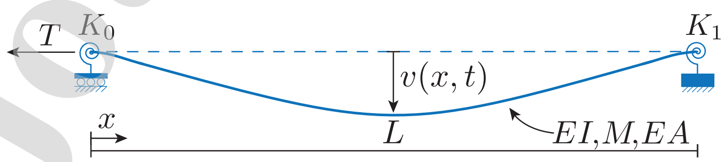

Figure 1: Structural model for an element of length L, with constant bending stiffness EI, axial stiffness EA and mass per unit length M, subjected to a tensile force $T > 0$ and restrained at its extremities by rotational springs of stiffness K_i. The subscripts $i = 0$ and $i = 1$ are respectively attributed to the left or the right end.

hinged, either perfectly clamped cable end sections (e.g. [7, 15, 14, 22]) but, in [21], the need for more refined boundary conditions, accounting for the rotational flexibility of the cable anchorages, is clearly pointed out. Definition of the rotational stiffness of the equivalent rotational springs strongly depends on the particular technology adopted to realize the restraints and is affected by different sources of uncertainties, such as those related to geometric imperfections and aging of the support devices. The rotational stiffness of the cable restraints, hence, should be added to the unknowns of the structural identification problem. The same modeling assumptions are also often adopted to identify the axial force of tie-rods in vaulted structural systems (e.g. [23, 40]).

However, whenever a significant dynamic interaction between a cable and the surrounding components is expected, such as for example in the case of cable trusses and nets, the proposed modeling strategy cannot be applied and different boundary conditions should be implemented (e.g. [41, 30]).

2.2. Dimensionless formulations

A reference length x_r and a reference time t_r are now employed to define the non-dimensional position, $\xi = x/x_r$, time, $\tau = t/t_r$, and transverse displacement of the cable centerline, $\nu(\xi,\tau) = v(x,t)/x_r$. The introduction of these new coordinates into the equation of motion provides the dimensionless form

$$\frac{EI}{T}\frac{1}{x_r^2}\,\partial_\xi^4\nu - \partial_\xi^2\nu + \frac{M}{T}\frac{x_r^2}{t_r^2}\,\partial_\tau^2\nu = 0. \tag{3}$$

The characteristic length is chosen as the length of the cable, $x_r = L$, while the characteristic time $t_r = 1/\Omega_r$ is chosen as the inverse of the fundamental frequency of a taut string

$$\Omega_r = \frac{1}{L}\sqrt{\frac{T}{M}} \tag{4}$$

in order to obtain a unitary coefficient in front of the time derivative. The dimensionless formulation of the equation of motion thus reads

$$\varepsilon^2\partial_\xi^4\nu - \partial_\xi^2\nu + \partial_\tau^2\nu = 0 \tag{5}$$

where $\xi \in [0,1]$, $\tau \in \mathbb{R}^+$ and $\varepsilon^2 = EI/TL^2$ is the bending stiffness parameter [42]. This dimensionless number is equal to zero for a taut string ($EI = 0$) and increases together with bending stiffness effects, when the structural element tends towards an Euler-Bernoulli beam by becoming shorter, less loaded or flexurally more rigid. In addition, the governing equation is singularly perturbed when ε is small since it multiplies the highest order space derivative, prefiguring the existence of boundary layers in the deformed shape of the cable [43, 44, 45]. In practice, ε is typically lower than 0.02 for slender structural elements, such as stay-cables [46], but belongs to the broader range $[0.02\,;1]$ for thicker structural elements, such as diagonal braces, truss bars, short hangers and tie-rods of historical vaulted structures [30, 29, 23, 47].

The boundary conditions are also dimensionlessly re-written as follows

$$\begin{cases} \nu\left(0,\tau\right)=0 \\ \nu\left(1,\tau\right)=0 \\ \varepsilon^2\partial_\xi^2\nu\left(0,\tau\right)-\kappa_0\partial_\xi\nu\left(0,\tau\right)=0 \\ \varepsilon^2\partial_\xi^2\nu\left(1,\tau\right)+\kappa_1\partial_\xi\nu\left(1,\tau\right)=0 \end{cases} \tag{6}$$

where $\kappa_i = K_i/TL$ are the non-dimensional rotational stiffness coefficients of the left $(i=0)$ and right $(i=1)$ springs. They take values in the left-bounded interval $[0,\infty[$ with hinged and clamped boundary conditions corresponding respectively to the zero lower bound value and to the infinite upper limit value. For modeling and identification purposes [28], the rotational degree-of-fixity parameters

$$\rho_i = \frac{\kappa_i}{\varepsilon+\kappa_i} \tag{7}$$

are preferred over the stiffness coefficients κ_i because their values lie in a closed unit interval $[0,1]$. Again, the lower and the upper bounds respectively correspond to the hinged $(\rho_i=0)$ and clamped $(\rho_i=1)$ boundary conditions.

2.3. Eigenproblem statement

By focusing on stationary oscillatory solutions [48], initial conditions are not required and, in the absence of external forcing, the transverse displacement can be expressed as the product of a mode shape function $\phi\left(\xi\right)$ and a time-dependent amplitude $q\left(\tau\right)$, according to the separation of variables method,

$$\nu\left(\xi,\tau\right)=\phi\left(\xi\right)q\left(\tau\right). \tag{8}$$

The partial differential equation of motion, Eq. (5), is consequently transformed into a set of two ordinary differential equations

$$\begin{cases} \ddot{q}+\omega^2\ q=0 \\ \varepsilon^2\ \phi''''-\phi''-\omega^2\ \phi=0 \end{cases} \tag{9}$$

where superscripted dots $\dot{}$ and apostrophes $'$ respectively denote differentiation with respect to τ and ξ. The first ODE shows that the time-dependent amplitude is given by

$$q\left(\tau\right)=q_0\sin\left(\omega\tau+\varphi\right) \tag{10}$$

where ω is the dimensionless circular frequency and φ is a constant phase shift depending on the initial conditions of the problem. The second ODE yields an expression for the mode shapes

$$\phi\left(\xi\right)=\mathbf{s}^T\mathbf{r} \tag{11}$$

where

$$\mathbf{r} = [r_1, r_2, r_3, r_4]^T \tag{12}$$

is the vector of integration constants and

$$\mathbf{s}(\xi) = [\sin(z_1\xi), \cos(z_1\xi), \exp(-z_2\xi), \exp(-z_2(1-\xi))]^T \tag{13}$$

is the vector of mode shape functions, in which

$$z_j = \frac{1}{\varepsilon\sqrt{2}}\sqrt{\sqrt{1+4(\omega\varepsilon)^2}+(-1)^j}\ ,\ j=(1,2)\,. \tag{14}$$

The last two components of the vector $\mathbf{s}$ are expressed with exponentials instead of hyperbolic sine and cosine functions to highlight the presence of boundary layers [43, 44, 45], developing near the left ($\xi \to 0^+$) and right ($\xi \to 1^-$) ends when $\varepsilon \ll 1$ and the supports are not pinned.

The substitution of Eq. (7), (8) and (10) in Eq. (6) gives

$$\begin{cases} \phi(0) = 0 \\ \phi(1) = 0 \\ (1-\rho_0)\,\varepsilon^2\phi^{''}(0) - \rho_0\varepsilon\phi^{'}(0) = 0 \\ (1-\rho_1)\,\varepsilon^2\phi^{''}(1) + \rho_1\varepsilon\phi^{'}(1) = 0 \end{cases} \tag{15}$$

for the boundary conditions and it is worth noting that the n-th order derivatives are always multiplied by the n-th power of ε thanks to the definition adopted for the degree-of-fixity parameters in Eq. (7). Besides, by setting $\rho_i = 0$ or $\rho_i = 1$, one consistently recovers the boundary condition relative to a hinged ($\phi^{''}(i) = 0$) or a clamped ($\phi'(i) = 0$) end.

Eq. (11) is then injected into the boundary conditions, yielding the following algebraic eigenvalue problem

$$\mathbf{B}\ \mathbf{r} = \mathbf{0} \tag{16}$$

where $\mathbf{0}$ is a four-row column vector and $\mathbf{B}$ is the boundary condition matrix

$$\mathbf{B} = \begin{pmatrix} 0 & 1 & 1 & e \\ s & c & e & 1 \\ -z_a\rho_0 & -z_a^2(1-\rho_0) & z_b^2(1-\rho_0)+z_b\rho_0 & ez_b^2(1-\rho_0)-ez_b\rho_0 \\ cz_a\rho_1 - sz_a^2(1-\rho_1) & -sz_a\rho_1 - cz_a^2(1-\rho_1) & ez_b^2(1-\rho_1)-ez_b\rho_1 & z_b^2(1-\rho_1)+z_b\rho_1 \end{pmatrix} \tag{17}$$

with

$$s = \sin(z_1)\ ;\ c = \cos(z_1)\ ;\ e = \exp(-z_2)\ ;\ z_a = \varepsilon z_1\ ;\ z_b = \varepsilon z_2.$$

The eigenproblem described by Eq. (16) is solved in two steps. Firstly, the eigenvalues ω_n, corresponding to the non-dimensional natural frequencies of the cable, are obtained by finding the roots of the determinant of the boundary conditions matrix

$$\det(\mathbf{B}) = 0 \tag{18}$$

and are thus functions of ε, ρ_0 and ρ_1. Since the matrix $\mathbf{B}$ involves trigonometric functions, Eq. (18) takes a transcendental form and admits countably infinite non-trivial solutions, $\omega_{n,k} \neq 0$ with $k \in \mathbb{N}^+$, as it is expected for a continuous structural element. Secondly, the eigenvalues provide inputs for the boundary conditions matrix and the solution of Eq. (16) gives the associated eigenvectors $\mathbf{r}_{n,k}$ (also called the vectors of integration constants).

2.4. Closed-form analytical solutions

In general, the zeros of Eq. (18) can be evaluated through any suitable root finding algorithm and, in this paper, the bisection method was successively applied to obtain them numerically, by using the dichotomy algorithm that has already been validated against a finite element model in [28]. However, in order to get a deeper understanding of the influence of each parameter on the dynamics of the cable, analytical formulas for the natural frequencies and the mode shapes are derived as well in the appendix. They are presented for cases of increasing complexity, starting from a doubly-hinged cable, which is the only configuration enabling to get exact closed-form expressions. Then, asymptotic solutions are derived for the small and the large natural frequencies of built-in and spring-supported elements whose bending stiffness parameter $\varepsilon \ll 1$. At the end, a composite approximation is obtained for the natural frequencies of a cable with partially restrained extremities by matching these asymptotic expressions. It reads

$$\omega_\rho^2 = (1 - \varepsilon\rho_r)^{-2} (k\pi)^2 + \varepsilon^2 (k\pi)^4 \tag{19}$$

where k is the mode number and $\rho_r = \rho_0 + \rho_1$ is the boundary condition parameter while the vectors of integration constants are asymptotically approached by

$$\mathbf{r}_\rho = \begin{pmatrix} 1 \\ -C \\ +C \\ \cos(z_1)\, C - \sin(z_1) \end{pmatrix} \tag{20}$$

with

$$C = \frac{\rho_0 z_a}{(1 - \rho_0)(z_a^2 + z_b^2) + \rho_0 z_b} \tag{21}$$

as detailed in the appendix.

2.5. Comments on the natural frequencies

For symmetry reasons, the natural frequencies are not modified by the swapping of ρ_0 and ρ_1. They are therefore foreseen to depend on symmetric combinations of these two degrees-of-fixity, such as their sum ρ_r which appears at leading order in Eq. (19) and satisfies the symmetry condition $\rho_r(\rho_0, \rho_1) = \rho_r(\rho_1, \rho_0)$. By introducing also $\rho_s = (\rho_0 - \rho_1)^2$, which is supposed to influence the natural frequencies at higher orders, the system of equation formed by ρ_r and ρ_s admits the two following pairs of solutions, for ρ_0 and ρ_1,

$$\left\{\begin{array}{lcl} 2\rho_0 & = & [1 \pm \alpha]\,\rho_r \\ 2\rho_1 & = & [1 \mp \alpha]\,\rho_r \end{array}\right. \quad \text{with} \quad \alpha = \sqrt{\frac{\rho_s}{\rho_r^2}} \tag{22}$$

that are characterised by the same natural frequencies.

Figure 2 illustrates the good agreement between the natural frequencies of a cable with intermediate rotational supports computed numerically or analytically, by means of Eq. (19). The results are presented for two different bending stiffness parameters, $\varepsilon = 0.05$ or $\varepsilon = 0.1$, and under four (ρ_r, ρ_s) pairs: (i) $\rho_r = 0$ and $\rho_s = 0$ ($\rho_0 = \rho_1 = 0$, doubly-hinged cable); (ii) $\rho_r = 2$ and $\rho_s = 0$ ($\rho_0 = \rho_1 = 1$, doubly-clamped cable); (iii) $\rho_r = 1$ and $\rho_s = 0$ ($\rho_0 = \rho_1 = 0.5$, same intermediate rigidity at both ends); (iv) $\rho_r = 1$ and $\rho_s = 0.36$ ($\rho_0 = 4\rho_1 = 0.8$ or equivalently $4\rho_0 = \rho_1 = 0.8$). In addition, they are compared to the outputs of the second-order accurate asymptotic expression

$$\omega_f^2 = (k\pi)^2 \left(1 + \varepsilon\rho_r + (\varepsilon\rho_r)^2 + \frac{1}{2}\varepsilon^2 (k\pi)^2\right)^2 \tag{23}$$

that has been developed to approximate the first few frequencies in [28] and generalizes the formula derived by Morse and Ingard for doubly-clamped cables [27], to account for a partial flexibility of the anchorages.

By looking at Figure 2 and by examining Eq. (19), it appears that the natural frequencies of a cable should follow two distinctive trends, depending on the mode number k, the bending stiffness parameter ε and the boundary conditions parameter ρ_r. Indeed, the second term of the sum in Eq. (19) is actually negligible compared to the first one when k is much smaller than $1/\left[(\pi\varepsilon)(1 - \varepsilon\rho_r)\right]$, and conversely. Far below this threshold, $\omega_\rho^2 \sim (1 - \varepsilon\rho_r)^{-2} (k\pi)^2$ and the natural frequencies grow like those of a taut string

$$\omega_t^2 = (k\pi)^2 \tag{24}$$

with a slope of 2 in log-log scale [19], as exhibited in Figure 2-(A). The ratios of ω_ρ^2/ω_t^2 presented in Figure 2-(B) are hence close to $(1 - \varepsilon\rho_r)^{-2}$ for the first few modes. At the opposite, for values of k far above $1/\left[(\pi\varepsilon)(1 - \varepsilon\rho_r)\right]$, $\omega_\rho^2 \sim \varepsilon^2 (k\pi)^4$ and the natural frequencies are approaching those of a simply-supported Euler-Bernoulli beam

$$\omega_b^2 = \varepsilon^2 (k\pi)^4 \tag{25}$$

with a slope of 4 in log-log scale [26], see Figure 2-(A,C). In that second asymptotic case, the reference numerical solution as well as the proposed composite solution also indicate that the natural frequencies are independent of the rotational stiffnesses at leading order.

Given that the range of validity of Eq. (23) is limited to small natural frequencies, it correctly fits the reference numerical solutions for small k but tends to drift as k increases. Indeed, Eq. (23) and Figure 2-(A) both show that

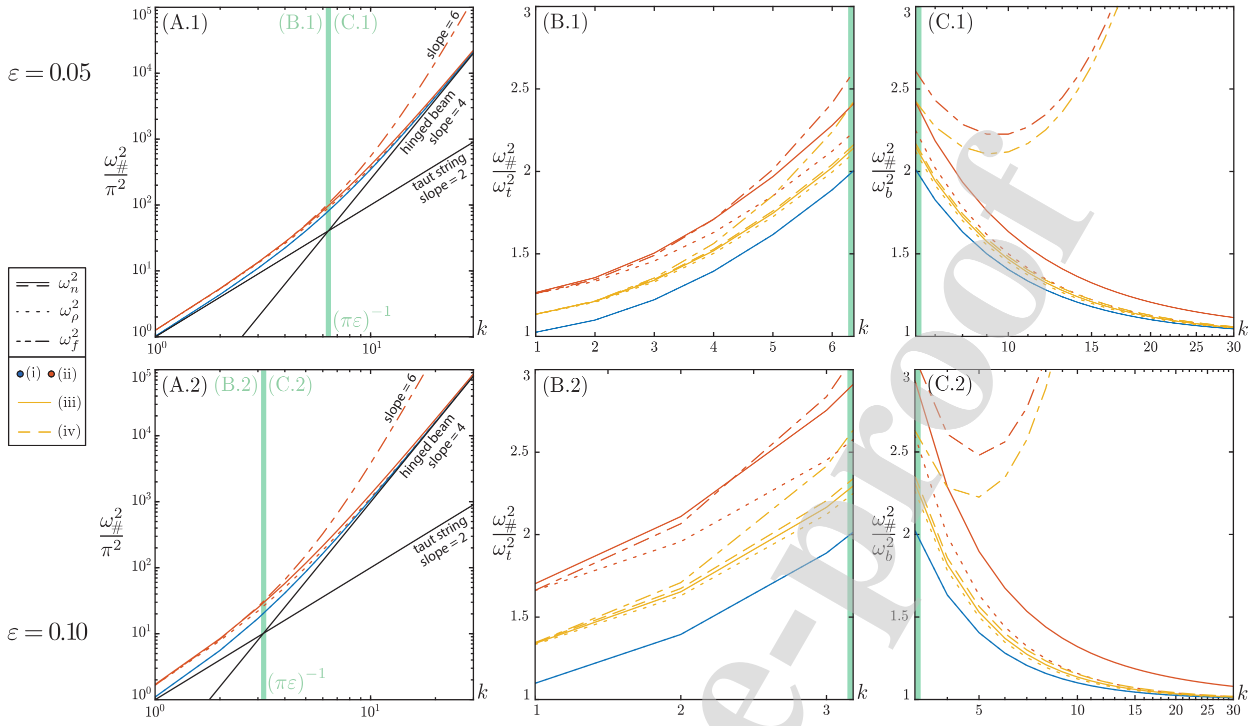

Figure 2: Comparison between the squared natural frequencies computed numerically, by means of a dichotomy algorithm [28], or analytically, with Eq. (19) and Eq. (23), as functions of the mode number k for two different values of the bending stiffness parameters, $\varepsilon = 0.05$ and $\varepsilon = 0.10$, and under four (ρ_r, ρ_s) pairs: (i) $(0, 0)$; (ii) $(2, 0)$; (iii) $(1, 0)$; (iv) $(1, 0.36)$. (A) Global picture. (B) In ratio with ω_t^2 from Eq. (24). (C) In ratio with ω_b^2 from Eq. (25). The subscript $\#$ refers to n, ρ or f depending on the line type, as indicated in the legend.

the squared natural frequencies ω_f^2 appropriately grow as k^2 for small k, while they increase as k^6 when $k \to \infty$, which is faster than the power law in k^4 expected for higher modes.

Last but not least, Eq. (19) ensures that the natural frequencies are, as always, increasing with the rigidity, whether it is due to the stiffening of the cable itself (ε) or of its end restraints (ρ_r), and that the exact limit cases of a taut string [19] or of a pinned-pinned cable [26] are easily recovered by setting either ε, either ρ_r, to zero, i.e. $\lim_{\varepsilon\rho_r \to 0^+} \left|\omega_\rho^2 - \omega_n^2\right| = 0$ and $\lim_{\varepsilon\rho_r \to 0^+} \left|\mathbf{r}_\rho - \mathbf{r}_n\right| = 0$. It thus gives Eq. (24) or

$$\omega_h^2 = (k\pi)^2 + \varepsilon^2 (k\pi)^4 \tag{26}$$

for the natural frequencies, respectively, and

$$\phi_s(\xi) = \sin(k\pi\xi) \tag{27}$$

for the mode shapes in both cases.

2.6. Comments on the mode shapes

Speaking of which, the mode shapes of taut strings and cables hinged at both ends are represented by black lines in Figure 3, along with the mode shapes of cables whose supports are characterized by three other pairs of rotational

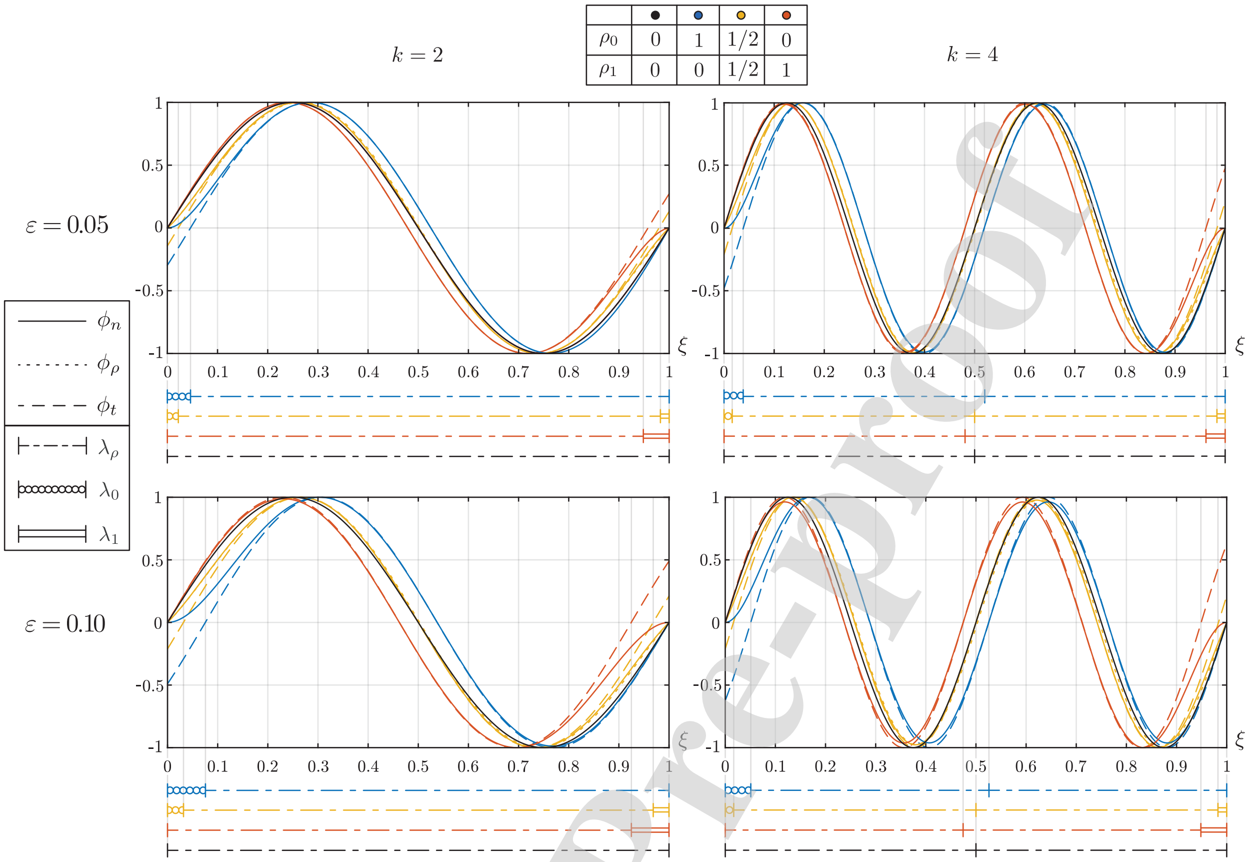

Figure 3: Comparison between the second and fourth mode shapes computed numerically, ϕ_n, by following the steps detailed in Section 2.3 or analytically, ϕ_ρ, by means of Eq. (28) for two different values of the bending stiffness parameters, $\varepsilon = 0.05$ and $\varepsilon = 0.10$, and under four (ρ_0, ρ_1) pairs: (i) $(0, 0)$; (ii) $(1, 0)$; (iii) $(1/2, 1/2)$; (iv) $(0, 1)$.

degrees-of-fixity: $(\rho_0, \rho_1) = (1, 0)$ in blue, $(\rho_0, \rho_1) = (1/2, 1/2)$ in yellow and $(\rho_0, \rho_1) = (0, 1)$ in orange. Just as Figure 2 for the natural frequencies, Figure 3 reveals an almost perfect fit between the mode shapes computed numerically or analytically by injecting Eq. (19) and Eq. (20) into Eq. (11):

$$\phi_\rho(\xi) = \sin(z_1 \xi) - C\cos(z_1 \xi) + C\exp(-z_2 \xi) + (\cos(z_1) C - \sin(z_1))\exp(-z_2(1-\xi)). \tag{28}$$

As shown in Figure 3 as well, the wavelength

$$\lambda_\rho = \frac{2\pi}{z_1} \tag{29}$$

of the sine and cosine functions encountered in Eq. (28) is shorter than those of a taut string or of a pinned-pinned cable

$$\lambda_s = \frac{2}{k} \tag{30}$$

when ε and ρ_r are both different from zero, since boundary layers develop at each non-hinged end of cables with small bending stiffness. Such a reduction of the wavelength is naturally (and mathematically, via z_1) consistent with the increase observed in the natural frequencies under the same conditions. This discrepancy regularly disappears as either ε, either ρ_r, tends to zero, i.e. $\lim_{\varepsilon\rho_r \to 0^+} |\lambda_\rho - \lambda_s| = 0$.

Aside from this global effect and interestingly enough, the mode shapes are also affected locally, through the vectors of integration constants, by the independent variation of each degree-of-fixity parameter and by their possible interchange, contrary to the natural frequencies. As a matter of fact, the first two terms of Eq. (28), involving sine and cosine functions of the same argument, can be merged to obtain the following expression

$$\phi_t(\xi) = \sqrt{1 + C^2}\sin(z_1\xi - \arctan(C)) \tag{31}$$

which outlines how the left boundary layer influences the mode shapes through the small bending stiffness parameter, i.e. when $0 < \varepsilon \ll 1$.

Indeed, if ρ_0 is different from zero, a boundary layer develops on the left end of the cable [45] because $C > 0$, just as the third integration constant. The mode shapes are therefore shifted to the right by a distance λ_0 equal to $\arctan(C)/z_1$ which is asymptotically approximated by $\varepsilon\rho_0$ for lower modes and tends towards zero for higher ones. Similarly, if ρ_1 is different from zero, a boundary layer emerges on the right end of the cable and extends over a distance equal to λ_1 as a result of the same wavelength reduction as mentioned before.

3. Inverse parameter identification problem

3.1. Minimal requirements

Most vibration-based identification procedures rely on a structural model and consist in updating its parameters until the error between the outcomes of its modal analysis and their experimental equivalents is minimized. In this paper, the structural model employed has been presented in Section 2. It is assumed that a set of dimensional natural frequencies Ω_{m,k_ω} and modal amplitudes $\phi_{m,k_\phi}(\xi_{k_\xi})$ at measurement positions ξ_{k_ξ}, with $k_\omega \in \mathbb{N}^+ \cap \{k_\omega \leq n_\omega\}$, $k_\phi \in \mathbb{N}^+ \cap \{k_\phi \leq n_\phi\}$ and $k_\xi \in \mathbb{N}^+ \cap \{k_\xi \leq n_\xi\}$, can be collected experimentally from transverse vibrations measured via standard dynamic testing techniques, since cables are typically light, slender, slightly damped and therefore easily excited by relatively small inputs of energy. Thanks to the simplicity of the expressions for the natural frequencies and the mode shapes introduced respectively in Eq. (19) and Eq. (28), the conclusions drawn in the previous section about the modal properties of a cable with arbitrary rotational end restraints are now exploited to provide some guidelines for the development of a method to identify the fundamental frequency $\tilde{\Omega}_r$, the bending stiffness parameter $\tilde{\varepsilon}$ and the rotational degrees-of-fixity, $\tilde{\rho}_0$ and $\tilde{\rho}_1$. Assuming that the length L and the mass per unit length M are known, these four numbers are subsequently employed to evaluate the tension $\tilde{T} = ML^2\tilde{\Omega}_r^2$ first, which is in turn used to determine the bending stiffness $\tilde{EI} = \tilde{T}L^2\tilde{\varepsilon}^2$ and the rotational stiffnesses $\tilde{K}_i = \tilde{T}L\tilde{\varepsilon}\tilde{\rho}_i/(1-\tilde{\rho}_i)$ of the cable. Irrespective of the bending stiffness and end conditions, any relative error Δ_M on the mass per unit length would result in a relative error $\Delta_T = \Delta_M$ on the identified tension and a relative error $\Delta_{EI} = \Delta_M$ on the bending stiffness [3].

In theory, it should be possible to get estimates for $\tilde{\Omega}_r$, $\tilde{\varepsilon}$, $\tilde{\rho}_r$ and $\tilde{\rho}_s$ on the sole basis of natural frequencies but, in practice, because of the smallness of ε, it is unrealistic to catch a third or fourth order detail like $\tilde{\rho}_s$ when the measured natural frequencies are corrupted by external noise and the model suffers from epistemic uncertainties. Moreover, the system of Eq. (22) potentially formed by $\tilde{\rho}_r$ and $\tilde{\rho}_s$ admits two solutions that prevent the attribution of a single value to each end restraint parameter, in compliance with the insensitivity of the natural frequencies to the swapping of $\tilde{\rho}_0$ and $\tilde{\rho}_1$.

In fact, according to Eq. (19), the squares of measured natural frequencies can be fitted properly by a second degree polynomial with only two terms at leading order, i.e. $a\,(k\pi)^2$ and $b\,(k\pi)^4$. Each of those two terms is leading over the other on a specific range of mode numbers and depends on the bending stiffness parameter. The first term, which is dominant for the first few frequencies, is also a function of the degree-of-fixity $\rho_r = \rho_0 + \rho_1$. Because there are only two terms or two coefficients, a and b, only two parameters out of three $(\Omega_r, \varepsilon, \rho_r)$ are identifiable from measured natural frequencies provided that the identification procedure relies upon (i) the first few natural frequencies, that are approximately given by the first term of the sum in Eq. (19) and should thus provide a correct estimation of the first-order coefficient, and (ii) a few natural frequencies whose mode numbers are close enough or even superior to the threshold value $1/\left[(\pi\varepsilon)\,(1-\varepsilon\rho_r)\right]$, in order to see the influence of the second term of the sum in Eq. (19), that grants access to the second-order coefficient of the polynomial. This observation therefore advises on which natural frequencies should enter, at least, into the objective function that has to be minimized through the updating process. As a corollary, to use only frequencies below the threshold $1/\left[(\pi\varepsilon)\,(1-\varepsilon\rho_r)\right]$ would not grant access to the coefficient of the second term, in b, and would result in a procedure that is able to identify only one out of the three parameters $(\Omega_r, \varepsilon, \rho_r)$.

Additional information coming from the identified mode shapes is then required to determine ρ_r or even more specifically ρ_0 and ρ_1. The closed form expression of the mode shapes indicates that they are divided into three parts at most, or more precisely one internal and two extremal parts, and that each of them is modified at leading order by different structural parameters. The internal part is defined by a sinusoidal function and gives access to the corresponding wavelength (affected by the bending stiffness), which is redundant with the natural frequencies via z_1 and z_2, while the extents of the boundary layers near the cable ends are asymptotically approached by $\varepsilon\rho_0$ and $\varepsilon\rho_1$ for the first few modes, respectively. Measurements of the modal displacements at both ends, that are associated to these first few mode numbers, thus provide the possibility to identify ρ_0 and ρ_1 independently. This requires the measurement points to be concentrated at the extremities of the cable, in the boundary layers, in order to capture λ_0 and λ_1. Besides, these distances shorten with increasing mode numbers. As a consequence, the first few modes, essentially, should be included in the identification procedure, for pratical reasons.

In brief, the recommendations for choosing which information should be considered in the identification are the following: use measurements of (i) the first few natural frequencies, (ii) a few natural frequencies whose mode order $k_\omega \geq 1/\pi\varepsilon$, (iii) the first few mode shapes, (iv) with measurement points located at both extremities of the cable, inside each boundary layer, i.e. $\xi \sim \varepsilon\rho_0$ and $\xi \sim (1-\varepsilon\rho_1)$ respectively.

3.2. Objective function

Within this context, the unknown parameters $\mathbf{x} = \{\Omega_r, \varepsilon, \rho_0, \rho_1\}$ can be identified by solving the nonlinear constrained optimization problem

$$\tilde{\mathbf{x}} = \underset{\mathcal{S}}{\operatorname{argmin}} \left[F_{\text{obj}}\left(\overline{\mathbf{x}}\right)\right] \tag{32}$$

in which the objective function F_{obj} reads

$$F_{\text{obj}}\left(\overline{\mathbf{x}}\right) = \frac{1}{n_\omega} \sum_{k_\omega=1}^{n_\omega} \left[1 - \frac{\Omega_{n,k_\omega}\left(\overline{\mathbf{x}}\right)}{\Omega_{m,k_\omega}\left(\mathbf{x}\right)}\right]^2 + \frac{1}{n_\phi}\frac{1}{n_\xi} \sum_{k_\phi=1}^{n_\phi} \sum_{k_\xi=1}^{n_\xi} \left[1 - \frac{\sigma_{n,k_\phi}\left(\xi_{k_\xi};\overline{\mathbf{x}}\right)}{\sigma_{m,k_\phi}\left(\xi_{k_\xi};\mathbf{x}\right)}\right]^2 \tag{33}$$

where the dimensional frequencies $\Omega_{n,k_\omega} = \Omega_r \omega_{n,k_\omega}$ are computed numerically and the relative modal displacements

$$\sigma_{\#,k_\phi}\left(\xi_{k_\xi}\right) = \frac{\phi_{\#,k_\phi}\left(\xi_{k_\xi}\right)}{\phi_{\#,k_\phi}\left(\xi_{\text{ref}}\right)} \tag{34}$$

are defined with respect to the reference displacement located at the position ξ_{ref}. The number of natural frequencies n_ω, the number of modes n_ϕ and the measurements positions ξ_{k_ξ} are selected in accordance with the guidelines listed above. Please notice that these requirements can be further reduced if one does not aim at determining simultaneously the four structural parameters, or if some of them are already known. In this case, the objective function can be modified accordingly, by removing the mode shapes if it is not necessary to identify the rotational end restraints for instance. Several applications available in the literature are particular cases of this general formulation; they are further discussed and analyzed in Section 3.5.

Finally, the vector of parameters subjected to the updating strategy $\overline{\mathbf{x}} = \left\{\overline{\Omega}_r, \overline{\varepsilon}, \overline{\rho}_0, \overline{\rho}_1\right\}$ is defined on the searching space $\mathcal{S}$, delimited by the physical constraints

$$\begin{cases} \tilde{\Omega}_c \leq \overline{\Omega}_r \leq \tilde{\Omega}_h \\ \tilde{\varepsilon}_h \leq \overline{\varepsilon} \leq \tilde{\varepsilon}_c \\ 0 \leq \overline{\rho}_0 \leq 1 \\ 0 \leq \overline{\rho}_1 \leq 1 \end{cases} \tag{35}$$

where

$$\left(\tilde{\Omega}_h, \tilde{\varepsilon}_h\right) = \underset{(\mathbb{R}^+,\mathbb{R}^+)}{\operatorname{argmin}} \left[F_{\text{obj}}\left(\left\{\overline{\Omega}_h, \overline{\varepsilon}_h, 0, 0\right\}\right)\right] \text{ and } \left(\tilde{\Omega}_c, \tilde{\varepsilon}_c\right) = \underset{(\mathbb{R}^+,\mathbb{R}^+)}{\operatorname{argmin}} \left[F_{\text{obj}}\left(\left\{\overline{\Omega}_c, \overline{\varepsilon}_c, 0, 0\right\}\right)\right] \tag{36}$$

are respectively the best fits obtained while assuming the cable to be hinged or clamped at both ends.

Although the traditional way to validate a new identification technique would be to demonstrate its applicability and robustness in various configurations, by including for instance some noise on simulated data or even by showing the realisticness of the results obtained with on site measurements, the goal of this paper is quite the opposite. It aims at establishing the minimum conditions to be fulfilled for the identification method to be fruitful. With this in mind, we chose to make some minimalistic noise corruption of the observations and study under which conditions the parameters of the identification method (e.g. number of modes, positions of sensors) **do not** allow a successful identification of the unknown mechanical parameters.

The assumed measured natural frequencies $\Omega_{m,k}$ are thus obtained by corrupting the outputs of the numerical model presented in Section 2.3 as follows,

$$\Omega_{m,k}(\mathbf{x}) = (1+\chi)\,\Omega_{n,k}(\mathbf{x}) \tag{37}$$

where $\chi \sim \mathcal{N}\left(0, I_n^2\right)$, i.e. is a zero-mean Gaussian noise with a low intensity, or standard deviation, I_n equal to 0%, 0.5% or 1% [3]. This approach is used in many other numerical studies [49, 50, 51, 52, 53] even though the intensity of the noises observed on natural frequencies determined through experimental or operational modal analysis is neither always constant over the mode ranks, nor always Gaussian [54, 55]. Nevertheless, it still allows to corrupt the natural frequencies, at least in a simple way, as desired.

Besides, it is decided to not corrupt the mode shapes whose measured values are then assumed to be given by

$$\phi_{m,k_\phi}\left(\xi_{k_\xi};\mathbf{x}\right) = \phi_{n,k_\phi}\left(\xi_{k_\xi};\mathbf{x}\right) \tag{38}$$

since the point of this paper is to derive necessary conditions to be met for the identification to be successful, as stated before. Contrary to the natural frequencies, adding independent Gaussian noises on each mode shape measurement without taking any spatial correlation into account is by no means realistic nor appropriate, as stated in [55]. To be in line with the current practices which recur to mode smoothing techniques (see e.g. [56]), one possibility to deal with experimental data among many others, including finite element model updating or low-pass filtering, is to assume that the measured mode shapes are correctly approximated by their asymptotic approximation, see Eq. (31) and to find the constant C that provides the best fit between measured and computed modal displacements. Then, a suitable manner to reproduce the effects of uncertainties that are correlated in space would be to corrupt the mode shapes by slightly and randomly modifying the constant C. These additional illustrations are not deemed essential to support the main message of this paper. The results obtained with such corrupted modal displacements are thus provided in the supplementary material.

As a prelude to the following investigations, the evolution of the objective function close to target parameters, $\mathbf{x} = \{5\ \mathrm{rad/s}, 0.06, 0.4, 0.6\}$, is represented in Figure 4 for a specific set of measurements, $k_\omega = \{1-15\}$, $k_\phi = \{1-3\}$ and $\xi_{k_\xi} = \{1,2,4\}\,\varepsilon/2 \cup 1-\{4,2,1\}\,\varepsilon/2$, which follows the recommendations enumerated in Section 3.1: the threshold frequency is $1/\pi\varepsilon = 5.3$, so there are (i) 5 natural frequencies below the threshold, (ii) 10 frequencies above the threshold, (iii) the first three mode shapes are used and (iv) their amplitude in the boundary layers are considered. The contours of the objective function show that the problem is well conditioned in the 4-dimensional searching space $\mathcal{S}$ and is characterized by a low sensitivity to noise. The specific shapes of the contours also reveal the existence of a single optimum.

By contrast, dropping any minimal requirement results in an ill-posed problem. In particular, when modal amplitudes are not measured at all, the topology of the objective function drastically changes, as shown in Figure 5. It appears to be far less sensitive to ε but to be much more affected by the noise than before, especially in the

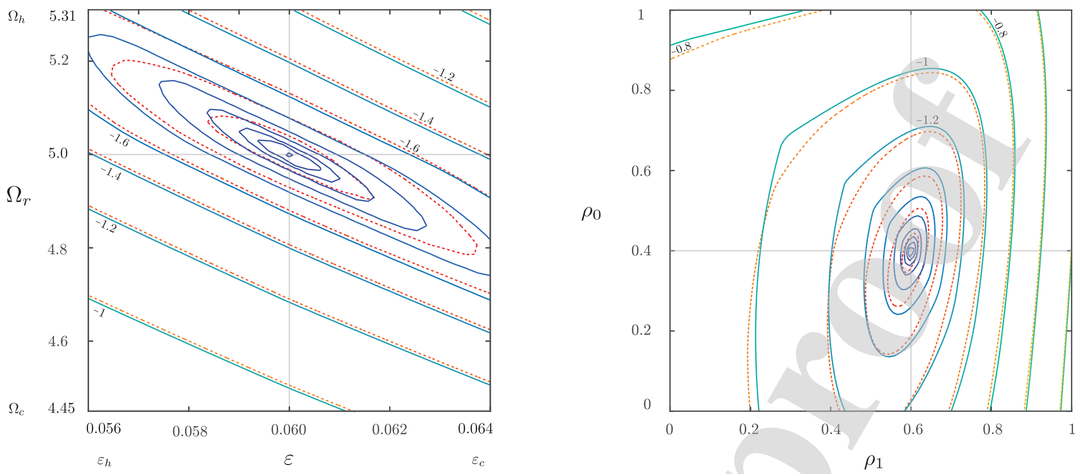

Figure 4: Contours of the objective function in log-scale around a given set of target parameters, $\mathbf{x} = \{5 \text{ rad/s}, 0.06, 0.4, 0.6\}$, when $k_\omega = \{1-15\}$, $k_\phi = \{1-3\}$ and $\xi = \{1, 2, 4\}\,\varepsilon/2 \cup 1 - \{4, 2, 1\}\,\varepsilon/2$. Blue-to-green plain lines and red-to-yellow dashed lines correspond respectively to different noise intensities, $I_n = 0\%$ and $I_n = 1\%$. Contours are spaced by a 0.2 difference in the decimal logarithm of the objective function.

plane $\rho_0 - \rho_1$ where the straight line $\rho_0 = \rho_1$ has in fact turned into an axis of symmetry. This is obviously in accordance with the insensitivity of the natural frequencies alone to the swapping of ρ_0 and ρ_1. Figure 5 finally demonstrates that ρ_r and ρ_s are clearly not identifiable as soon as the noise intensity is different from zero since it completely flattens the objective function in a large area, see dashed lines, while two minima take place in the absence of noise.

3.3. Differential Evolution

In this paper, a custom implementation of the Differential Evolution (DE) algorithm introduced by Storn and Price [57], belonging to the family of improved variants proposed by [58], has been implemented in order to find the set of parameters that minimizes the objective function presented in Eq. (33) and, as a result, solve the nonlinear constrained optimization problem presented in Eq. (32). As it is well known [59], gradient-free algorithms like DE are particularly well suited to deal with cost functions that are not very sensitive to some input parameters or that are likely to exhibit several local minima, as it is the case for the objective function at hand, which is almost indifferent to modifications of the degree-of-fixity parameters for small values of the bending stiffness parameter ε and contains local minima as soon as unavoidable measurement errors affect the modal characteristics of the cable.

In more details, DE is an Evolutionary Algorithm operating on a population of N candidate solution vectors to make it evolve over the iterations and eventually converge towards a target vector which globally minimizes the objective function. As illustrated in Figure 6, a typical run for a cable characterized by the vector of parameters $\mathbf{x} = \{5 \text{ rad/s}, 0.06, 0.4, 0.6\}$ starts with an initial population composed of $\left(N - 2^4\right)$ elements (blue dots in Figure 6) which are randomly chosen within the searching space $\mathcal{S}$, as usual, and 2^4 elements (red dots in Figure 6) which are especially imposed here to cover the full range of parameters, as indicated in Eq. (35), in order to ensure that

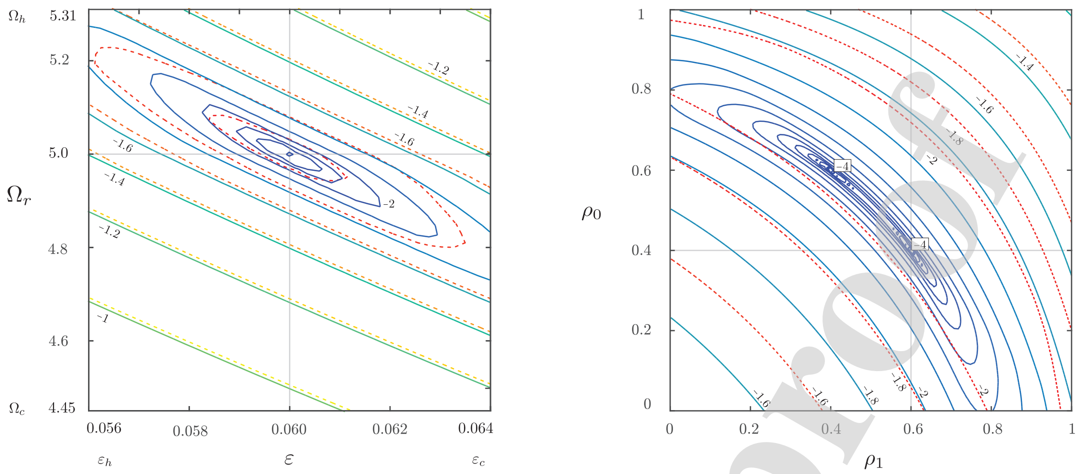

Figure 5: Contours of the objective function in log-scale around a given set of target parameters, $\mathbf{x} = \{5 \text{ rad/s}, 0.06, 0.4, 0.6\}$, when $k_\omega = \{1-15\}$, $k_\phi = \varnothing$ and $\xi_{k_\xi} = \varnothing$. Blue-to-green plain lines and red-to-yellow dashed lines correspond respectively to different noise intensities, $I_n = 0\%$ and $I_n = 1\%$. Contours are spaced by a 0.2 difference in the decimal logarithm of the objective function.

the algorithm is able to head towards the boundaries of the searching space $\mathcal{S}$.

Then, offsprings are generated by perturbing the current population with scaled differences of randomly selected elements and the new population is the result of a one-to-one parent/offspring competition based on the value of the objective function associated to each candidate. The physical constraints can thus be enforced by allocating a penalty to the elements that do not fulfill the conditions described in Eq. (35) and iterations are performed until the final population (turquoise dots in Figure 6) satisfies at least one of the following termination criteria: (a) the cost function of the best member is lower than the prescribed value OBJ, (b) the relative difference between the objective functions corresponding to the best and worst members of the population is below a given threshold named TOL [60], (c) the number of iterations NIT reaches its specified maximum value $MAXIT$.

For instance, the convergence of the algorithm during a typical run is depicted in Figure 7. A cable is supposed to be described by the vector of parameters $\mathbf{x} = \{5 \text{ rad/s}, 0.06, 0.4, 0.6\}$ again and intermediate parameter estimates associated to the member with the lowest cost function, i.e. the best member, are displayed for each iteration NIT, together with the values that have to be compared to OBJ and TOL in order to stop the iterative procedure.

3.4. Numerical verification

While Figure 6 and Figure 7 show the initial and final populations, but also the results obtained for a single set of target parameters, Figure 8 and Figure 9 respectively gather the errors made on the four direct $\left(\tilde{\Omega}_r, \tilde{\varepsilon}, \tilde{\rho}_0, \tilde{\rho}_1\right)$ and indirect $\left(\tilde{T}, \tilde{EI}, \tilde{K}_0, \tilde{K}_1\right)$ outputs of the identification procedure obtained for many configurations by running DE with a number of initial candidate vectors $N = 40$, a scale factor $F = 0.8$, a crossover parameter $CR = 0.9$, see [59] for further explanations, and the termination criteria: $TOL = 5.10^{-4}$, $OBJ = 10^{-4}$ and $MAXIT = 250$ which are responsible for the small errors represented in Figure 8 and Figure 9 when $I_n = 0\%$. These values have been

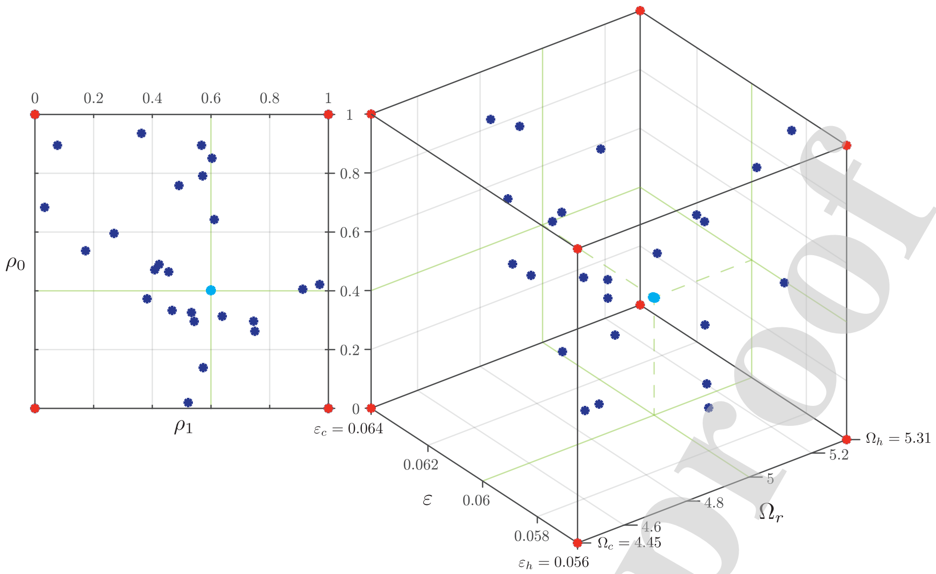

Figure 6: Illustration of the searching space and distribution of the initial (blue and red dots) and final (turquoise dots) populations associated to a typical run of DE for a cable whose target parameters are represented by green lines. The initial population is composed of randomly chosen elements, in blue, and elements on the boundary of the searching space, in red.

chosen loose enough to guarantee that the iterative procedure never ends because of the criterion (c), as is well the case in Figure 7 where criterion (a) or criterion (b) are respectively fulfilled when the noise intensity is either equal to zero, either equal to one percent.

In the extensive examples, the fundamental frequency Ω_r is always fixed at 5 rad/s and two different bending stiffness parameters, $\varepsilon = 0.03$ ($1/\pi\varepsilon = 10.6$) and $\varepsilon = 0.06$ ($1/\pi\varepsilon = 5.3$), are considered along with six different values for each rotational degree-of-fixity parameter: $0, 0.2, 0.4, 0.6, 0.8$ and 1. The objective function included 15 natural frequencies, 3 mode shapes and 3 measurement points at each end of the cable, positioned at the dimensionless coordinates $\xi = \{1, 2, 4\}\,\varepsilon/2$ and $\xi = 1 - \{4, 2, 1\}\,\varepsilon/2$. This specific choice of measurements ensures that the guidelines provided before are all followed, no matter the value of the bending stiffness parameter, since $n_\omega = 15$ is greater than $\max(10.6; 5.3)$.

Figure 8 and Figure 9 demonstrate that DE globally delivers accurate estimates for the fundamental frequency and for the bending stiffness parameters, with respectively less than 1.1% and 1.7% relative errors, all cases considered. They can be used to get accurate estimates of the axial force and the flexural rigidity of the structural element, with respectively less than 2.2% and 2.7% absolute relative errors. It seems interesting to notice here that the relative error on the axial force

$$\Delta_T = \frac{\tilde{T}}{T} - 1 \tag{39}$$

is approximately twice the relative error on the fundamental frequency

$$\Delta_\Omega = \frac{\tilde{\Omega}_r}{\Omega_r} - 1 \tag{40}$$

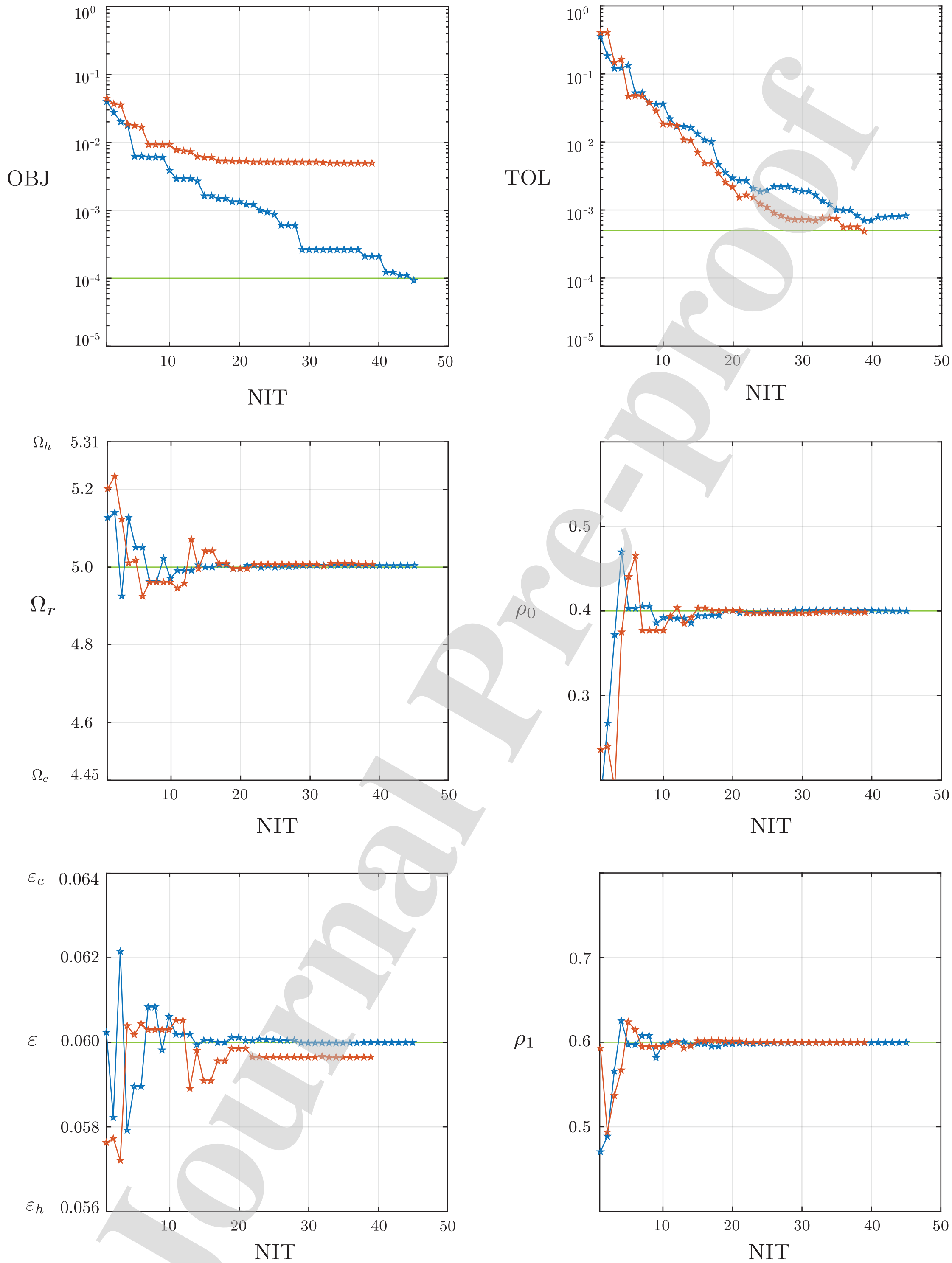

Figure 7: Convergence of the iterative procedure during a typical run of the DE algorithm for a cable whose target parameters are represented by green lines. Blue and red stars are respectively associated to a noise intensity of 0% or 1% on the natural frequencies.

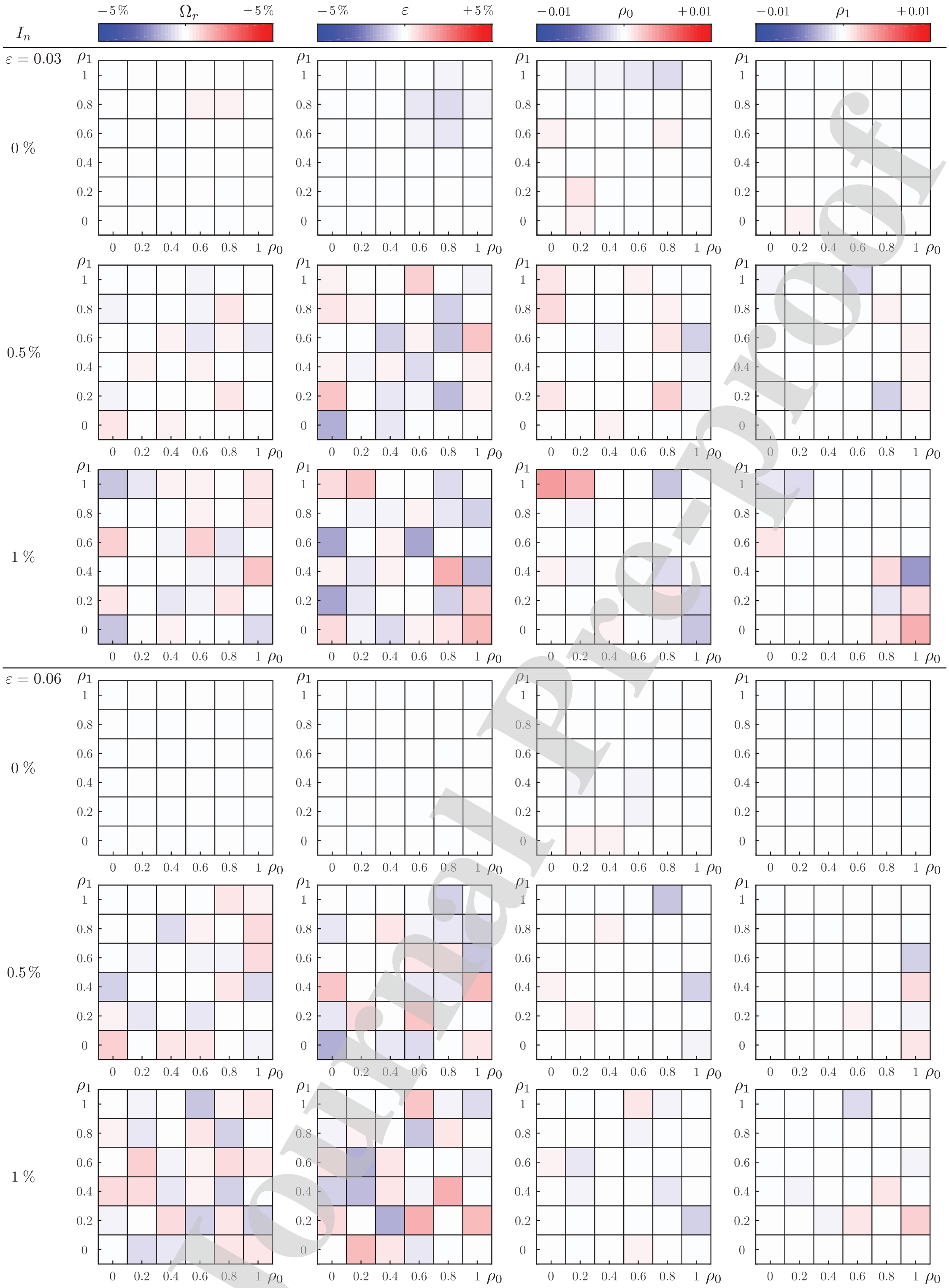

Figure 8: Relative or absolute errors between the target parameters and the values obtained by the identification procedure for three different values of the noise intensity ($I_n = 0\%$, $I_n = 0.5\%$ and $I_n = 1\%$), two different values of the bending stiffness parameter ($\varepsilon = 0.03$ and $\varepsilon = 0.06$) and six different values of each degree-of-fixity parameter $(0, 0.2, 0.4, 0.6, 0.8$ and $1)$. Absolute errors are considered for the degrees-of-fixity because their reference value is equal to zero in some cases.

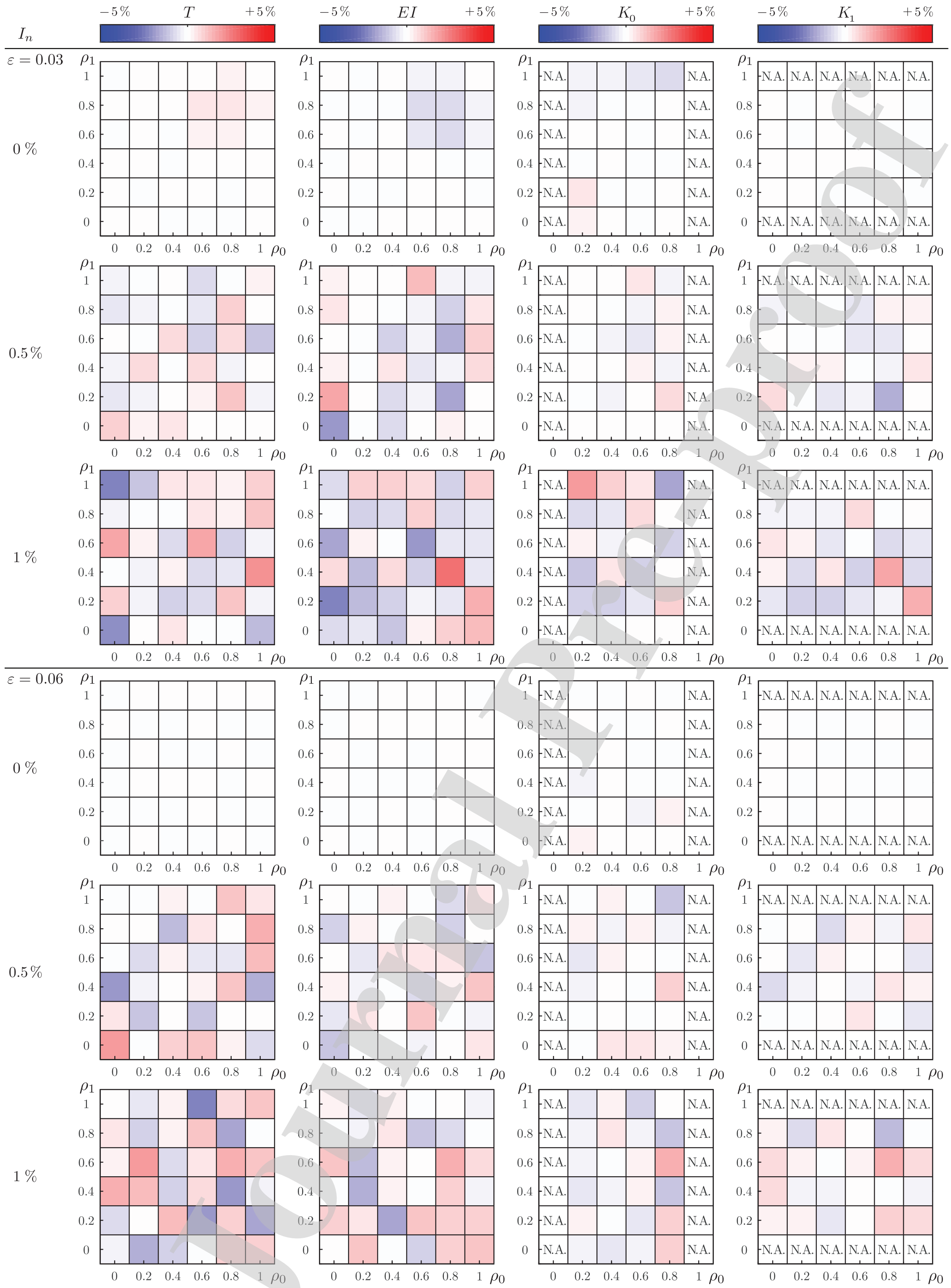

Figure 9: Relative errors between the target parameters and the values obtained by the identification procedure for three different values of the noise intensity ($I_n = 0\%$, $I_n = 0.5\%$ and $I_n = 1\%$), two different values of the bending stiffness parameter ($\varepsilon = 0.03$ and $\varepsilon = 0.06$) and six different values of each degree-of-fixity parameter ($0, 0.2, 0.4, 0.6, 0.8$ and 1). Relative errors cannot be computed (N.A.) when the reference value is equal to zero or goes towards infinity.

when those errors are small since it is possible to show that

$$\Delta_T = 2\Delta_\Omega + \Delta_\Omega^2 \tag{41}$$

after some straightforward manipulations of Eq. (4), see also [3].

Nevertheless, as it can be clearly appreciated from Figure 8 and Figure 9 again, DE also correctly determines the two degree-of-fixity parameters, ρ_0 and ρ_1, with less than 0.004 absolute error, all cases considered, and thus the rotational rigidities, K_0 and K_1, with less than 1% relative error. This estimator applies to cases for which the support stiffnesses are neither equal to zero, nor going towards infinity.

These numerical examples therefore confirm that all four parameters of the problem (Ω_r, ε, ρ_0 and ρ_1 or their equivalent dimensional quantities T, EI, K_0 and K_1) can be precisely estimated in this context by using the Differential Evolution algorithm once the recommendations concerning the choice of measurements that have to be incorporated in the objective function are followed. Although it does not allow to conclude that such a procedure would perform equally well with more realistic examples, it certifies that any important loss of accuracy occurring after a change in the objective function cannot be attributed to the algorithm.

3.5. Challenging the guidelines

The second part of the demonstration, hence, consists in showing that the identification fails if at least one of the requirements is not fulfilled. The literature shows that existing methods indeed struggle in these circumstances, as briefly detailed next.

First, methods that do not include any measurement of the mode shapes are only able to identify two independent parameters; and this is also conditioned upon small noise on measured natural frequencies. For instance, in [8], the axial force and a global rotational stiffness (equivalent of ρ_r) have been correctly identified because the bending stiffness was known in advance while, in [28], ρ_r was fixed to a pragmatic value in order to determine the fundamental frequency and the bending stiffness parameter. These observations are corroborated in this paper as well by looking at Figure 4 and Figure 5, which illustrate the evolution of the objective function close to a given set of target parameters when modal amplitudes are included in the measurements or are not considered at all, respectively. Indeed, in the latter case, the problem is clearly not well conditioned.

Then, by adding a single piece of data relative to the mode shapes as in [21], it became possible to determine a global rotational stiffness as well; but not each rotational end restraint, separately, because measurements in the distinctive boundary layers were omitted. It clearly underpins the importance of the fourth guideline.

In an alternative approach, when dealing with one natural frequency and at least five associated modal displacements, see [29], the wavelength and the extent of the two boundary layers have been accurately evaluated provided some measurement positions were close enough to the extremities of the element. It thus gave the possibility to adjust three parameters (T, K_0 and K_1) whereas the value of the fourth one (EI) had to be defined apart. The uniform distribution of sensors recommended in that paper explains however why the method fails when the bending stiffness parameter is too small. In fact, the size of the boundary layers decreases with ε, the measurement positions hence fall out of these zones and information about the boundary conditions are lost. Again, this shows the importance of the fourth guideline.

Although they are fully supported by the above mathematical analysis, the importance of each specific guideline is hence also observable thanks to evidences coming from the literature. They are further complemented by means of additional numerical simulations summarized in Figure 10. This figure shows the dispersion of the results of the identification obtained over 100 runs of a noised version (I_n =1%) of the following nominal case: the fundamental frequency Ω_r is equal to 5 rad/s, the bending stiffness parameter is fixed at 0.03 and the rotational degree-of-fixity parameters, ρ_0 and ρ_1, are respectively 0.2 and 0.8, while the previous set of measurements is taken as a reference and is modified in one way among the four following:

(i) the number of natural frequencies is reduced, i.e. $k_\omega = \{1, 2, ..., n_\omega\}$ with $n_\omega = 15$, 10 or 5;

(ii) the first five natural frequencies and the 6$^{\text{th}}$, the 8$^{\text{th}}$ or the 10$^{\text{th}}$ one are selected;

(iii) displacements in the 1$^{\text{st}}$, the 4$^{\text{th}}$ or the 8$^{\text{th}}$ mode shape only are considered;

(iv) sensors are positioned near the left end only, $\xi_{k_\xi} = \{1, 2, 4\}\,\varepsilon/2$, or the right end only, $\xi_{k_\xi} = 1 - \{4, 2, 1\}\,\varepsilon/2$.

The boxplots contained in the first column of Figure 10 demonstrate that the identification is more accurate when the number of frequencies increases, as expected. However, by comparing the results obtained when $k_\omega = \{1 - 10\}$ to those obtained when $k_\omega = \{1 - 5\} \cup \{10\}$, in the second column of the Figure, it appears that the same level of precision can be approximately reached even though there is a gap in the list of the natural frequencies considered in the latter case. It thus demonstrates the usefulness of the first and the second guidelines which advise to rely on the first few natural frequencies, but also on some natural frequencies related to sufficiently high modes. As a consequence, instead of trying to measure a lot of natural frequencies, it seems more interesting to focus on the detection of the appropriate ones: a few below and a few above the threshold.

Similarly, the results presented in the third column of Figure 10 indicate that the fourth mode is already too high to be regarded as one of the first few modes mentioned in the third guideline because it does not allow to get correct estimates for the degree-of-fixity parameters, unlike the very first one. Nevertheless, it seems necessary to point out that it might depend on the measurement positions too. Indeed, the shortening of the boundary layers with increasing mode numbers could certainly be compensated by zooming even more on the extremities of the element if one is able to do so in practice and measurements of modal displacements in higher modes could thus be useful.

At last, as displayed in the fourth column of Figure 10, the procedure fails at identifying ρ_0 when the measurement positions are concentrated near the right end of the element but conversely delivers an accurate estimate for ρ_1. This is due to the fact that the target value (0.2) of ρ_0 is much lower than that (0.8) of ρ_1 and is hence not easily indirectly identifiable while the value of ρ_1 can be correctly determined once ρ_r and ρ_0 are obtained by using measurements of modal amplitudes in the left boundary layer. Since the opposite might as well occur, the fourth guideline makes perfect sense and measurements should accordingly be positioned on both sides of the elements, inside each boundary layer, in order to estimate the degree-of-fixity parameters.

Figure 10: Distribution of the results obtained at the end of the identification procedure for 100 sets of noisy natural frequencies ($I_n = 1\%$) and modal amplitudes, generated numerically. The measurements included in the objective function differ in each column: (1) $k_\omega = \{1 - n_\omega\}$ with $n_\omega = 5$, 10 or 15, $k_\phi = \{1 - 3\}$ and $\xi_{k_\xi} = \{1, 2, 4\}\,\varepsilon/2 \cup 1 - \{4, 2, 1\}\,\varepsilon/2$, (2) $k_\omega = \{1 - 5\} \cup \{k_+\}$ with $k_+ = 6$, 8 or 10, $k_\phi = \{1 - 3\}$ and $\xi_{k_\xi} = \{1, 2, 4\}\,\varepsilon/2 \cup 1 - \{4, 2, 1\}\,\varepsilon/2$, (3) $k_\omega = \{1 - 15\}$, $k_\phi = 1$, 4 or 8 and $\xi_{k_\xi} = \{1, 2, 4\}\,\varepsilon/2 \cup 1 - \{4, 2, 1\}\,\varepsilon/2$, (4) $k_\omega = \{1 - 15\}$, $k_\phi = \{1 - 3\}$ and $\xi_{k_\xi} = \{1, 2, 4\}\,\varepsilon/2$ or $1 - \{4, 2, 1\}\,\varepsilon/2$ or both. The red lines correspond to the median values, the blue boxes extend from the 25$^{\text{th}}$ to the 75$^{\text{th}}$ percentiles and the edges of the whiskers represent the minimum and maximum values encountered, respectively.

4. Conclusions

All in all, this paper proves that any identification procedure whose objective function does not include measurements of (i) the first few natural frequencies, (ii) a first few natural frequencies associated to higher modes ($k_\omega \sim 1/\pi\varepsilon$) and (iii) several modal displacements in the first few mode shapes (iv) located in each boundary layer, whose extent scale with $\varepsilon\rho_i$, fails at the simultaneous identification of the axial force, the bending stiffness and the rotational end restraints.

These minimal requirements have been derived from the closed-form asymptotic expressions that are established in this paper for the natural frequencies and the mode shapes of a highly tensioned cable with a small bending stiffness anchored to supports that are neither hinges, nor clamps, but rather in between.

5. Appendix

5.1. Hinged boundary conditions, $\rho_0 = 0$ and $\rho_1 = 0$

The particular case of a doubly-hinged cable is the only configuration for which it is possible to determine the exact closed-form expression of the natural frequencies. As $\rho_0 = 0$ and $\rho_1 = 0$, the boundary conditions matrix reads

$$\mathbf{B}_h = \begin{pmatrix} 0 & 1 & 1 & e \\ s & c & e & 1 \\ 0 & -(\varepsilon z_1)^2 & (\varepsilon z_2)^2 & e(\varepsilon z_2)^2 \\ -s(\varepsilon z_1)^2 & -c(\varepsilon z_1)^2 & e(\varepsilon z_2)^2 & (\varepsilon z_2)^2 \end{pmatrix} \tag{42}$$

and its determinant cancels out if $\sin(z_1) = 0$. The well-known formula

$$\omega_h^2 = (k\pi)^2 + \varepsilon^2 (k\pi)^4 \tag{43}$$

therefore provides the natural frequencies of a cable hinged at both ends [26].

5.2. Clamped boundary conditions, $\rho_0 = 1$ and $\rho_1 = 1$

For a cable clamped at both ends, as $\rho_0 = 1$ and $\rho_1 = 1$, the boundary conditions matrix becomes

$$\mathbf{B}_c = \begin{pmatrix} 0 & 1 & 1 & e \\ s & c & e & 1 \\ -\varepsilon z_1 & 0 & \varepsilon z_2 & -e\varepsilon z_2 \\ c\varepsilon z_1 & -s\varepsilon z_1 & -e\varepsilon z_2 & \varepsilon z_2 \end{pmatrix} \tag{44}$$

and its determinant is equal to zero when

$$\left(1 - e^2\right)\sin(z_1) - 2\omega\varepsilon\left(1 + e^2\right)\cos(z_1) + 4\omega\varepsilon e = 0. \tag{45}$$

Contrary to the hinged configuration, it is not possible to provide a simple but exact expression for the natural frequencies of a doubly-clamped cable because the transcendental equation deriving from the cancellation of the determinant is too complex to be solved analytically as such.

Nevertheless, the asymptotic solutions

$$\omega_u^2 = (1-2\varepsilon)^{-2}(k\pi)^2 \text{ or } \omega_v^2 = \varepsilon^2 (k\pi)^4 \tag{46}$$

can be found for small or large frequencies when $\varepsilon \ll 1$, by keeping the leading order terms in the series expansions of z_1 and z_2 for $\omega\varepsilon \ll 1$ or $\omega\varepsilon \gg 1$, respectively, and by neglecting the resulting exponentially small terms. The natural frequencies of a built-in cable can then be compositely approximated by

$$\omega_c^2 = \omega_u^2 + \omega_v^2 \tag{47}$$

since each term is leading over the other on the specific range of mode numbers where it is supposed to match correctly the frequencies.

5.3. Intermediate boundary conditions, $\rho_0 \in]0,1[$ and $\rho_1 \in]0,1[$

Similarly to the clamped case, the composite approximation of the natural frequencies of a cable with intermediate rotational end restraints is expressed as

$$\omega_\rho^2 = (1-\varepsilon\rho_r)^{-2}(k\pi)^2 + \varepsilon^2 (k\pi)^4 \tag{48}$$

where

$$\rho_r = \rho_0 + \rho_1 \tag{49}$$

by conserving the leading order terms in the series expansions of z_1 and z_2 for $\omega\varepsilon \ll 1$ or $\omega\varepsilon \gg 1$ and by discarding the exponentially small ones on the basis that $\varepsilon \ll 1$.

5.4. Vectors of integration constants

The leading order term in the series expansion of z_2 for $\omega\varepsilon \ll 1$ or $\omega\varepsilon \gg 1$ is respectively equal to $1/\varepsilon$ or $\sqrt{\omega/\varepsilon}$. Therefore, $\exp(-z_2)$ is negligible in both asymptotic cases when $\varepsilon \ll 1$. The boundary conditions matrix thus reads

$$\mathbf{B}_\rho = \begin{pmatrix} 0 & 1 & 1 & 0 \\ s & c & 0 & 1 \\ -z_a\rho_0 & -z_a^2(1-\rho_0) & z_b^2(1-\rho_0)+z_b\rho_0 & 0 \\ cz_a\rho_1 - sz_a^2(1-\rho_1) & -sz_a\rho_1 - cz_a^2(1-\rho_1) & 0 & z_b^2(1-\rho_1)+z_b\rho_1 \end{pmatrix} \tag{50}$$

for a cable with intermediate boundary conditions. The vectors of integration constants are then obtained as follows

$$\mathbf{r}_\rho = \begin{pmatrix} 1 \\ -C \\ +C \\ \cos(z_1)\, C - \sin(z_1) \end{pmatrix} \tag{51}$$

where

$$C = \frac{\rho_0 z_a}{(1-\rho_0)\left(z_a^2 + z_b^2\right) + \rho_0 z_b} \tag{52}$$

without any further approximation.

Acknowledgements

The work of the first author, M. Geuzaine, is supported by the National Research Fund for Scientific Research of Belgium (F.R.S.-FNRS) through a FRIA grant. This research work has also been partly funded by the Walloon Public Services (SPW, Service Public de Wallonie).

[1] J. M. Ko, Y. Q. Ni, H. F. Zhou, J. Y. Wang, and X. T. Zhou. Investigation concerning structural health monitoring of an instrumented cable-stayed bridge. *Structure and Infrastructure Engineering*, 2009.

[2] João P. Santos, Christian Crémona, Luís Calado, Paulo Silveira, and André D. Orcesi. On-line unsupervised detection of early damage. *Structural Control and Health Monitoring*, 2016.

[3] Elsa de Sá Caetano, International Association for Bridge, and Structural Engineering. *Cable Vibrations in Cable-stayed Bridges*. Structural engineering documents. IABSE, 2007.

[4] S. Kangas, A. Helmicki, V. Hunt, R. Sexton, and J. Swanson. Cable-stayed bridges: Case study for ambient vibration-based cable tension estimation. *Journal of Bridge Engineering*, 17(6):839–846, 2012.

[5] Jean Paul Gourmelon. Fatigue des câbles de haubanage: Organisation et principaux résultats du programme de recherche dirigé par le LCPC. *Bulletin des Laboratoires des Ponts et Chaussees*, (244-245):53–71, 2003.

[6] D Siegert and P Brevet. Fatigue of stay cables inside end fittings: high frequencies of wind induced vibrations. *Bulletin-International Organisation for the Study of the Endurance of Ropes*, 89:43, 2005.

[7] Armin B. Mehrabi. In-service evaluation of cable-stayed bridges, overview of available methods and findings. *Journal of Bridge Engineering*, 11(6):716–724, 2006.

[8] Timothy Kernicky, Matthew Whelan, and Ehab Al-Shaer. Dynamic identification of axial force and boundary restraints in tie rods and cables with uncertainty quantification using Set Inversion Via Interval Analysis. *Journal of Sound and Vibration*, 423:401–420, 2018.

[9] Habib Tabatabai. *Inspection and Maintenance of Bridge Stay Cable Systems.* Transportation Research Board of the National Academies, Washington, 2005.

[10] X. G. Hua, Y. Q. Ni, Z. Q. Chen, and J. M. Ko. Structural damage detection of cable-stayed bridges using changes in cable forces and model updating. *Journal of Structural Engineering*, 135(9):1093–1106, 2009.

[11] Paolo Clemente, Giovanni Bongiovanni, Giacomo Buffarini, and Fernando Saitta. Structural health status assessment of a cable-stayed bridge by means of experimental vibration analysis. *Journal of Civil Structural Health Monitoring*, 2019.

[12] Byeong Hwa Kim and Taehyo Park. Estimation of cable tension force using the frequency-based system identification method. *Journal of Sound and Vibration*, 304(3-5):660–676, jul 2007.

[13] Soojin Cho, Jinsuk Yim, Sung Woo Shin, Hyung Jo Jung, Chung Bang Yun, and Ming L. Wang. Comparative field study of cable tension measurement for a cable-stayed bridge. *Journal of Bridge Engineering*, 18(8):748–757, 2013.

[14] Chiara Bedon, Michele Dilena, and Antonino Morassi. Ambient vibration testing and structural identification of a cable-stayed bridge. *Meccanica*, 51(11):2777–2796, 2016.

[15] Francesco Benedettini and Carmelo Gentile. Operational modal testing and FE model tuning of a cable-stayed bridge. *Engineering Structures*, 2011.

[16] Xuefeng Zhao, Kwang Ri, and Niannian Wang. Experimental Verification for Cable Force Estimation Using Handheld Shooting of Smartphones. *Journal of Sensors*, 2017, 2017.

[17] Banfu Yan, Wenbing Chen, Jiayong Yu, and Xiaomo Jiang. Mode shape-aided tension force estimation of cable with arbitrary boundary conditions. *Journal of Sound and Vibration*, 440:315–331, 2019.

[18] Ph De Mars and D Hardy. Mesure des efforts dans les structures à câbles. *Annales des travaux publics de Belgique*, 6:515–531, 1985.

[19] A Preumont. *Twelve Lectures on Structural Dynamics*, volume 198. 2013.

[20] H.M. Irvine and T.K. Caughey. The linear theory of free vibrations of a suspended cable. *Proceedings of the Royal Society of London*, 341(1626):299–315, 1974.

[21] Marcelo A. Ceballos and Carlos A. Prato. Determination of the axial force on stay cables accounting for their bending stiffness and rotational end restraints by free vibration tests. *Journal of Sound and Vibration*, 317(1-2):127–141, oct 2008.

[22] R. Geier, G. De Roeck, and R. Flesch. Accurate cable force determination using ambient vibration measurements. *Structure and Infrastructure Engineering*, 2(1):43–52, 2006.

[23] Sergio Lagomarsino and Chiara Calderini. The dynamical identification of the tensile force in ancient tie-rods. *Engineering Structures*, 27(6):846–856, 2005.

[24] Yong Hui Huang, Ji Yang Fu, Rong Hui Wang, Quan Gan, and Ai Rong Liu. Unified practical formulas for vibration-based method of cable tension estimation. *Advances in Structural Engineering*, 18(3):405–422, 2015.

[25] Sheng Hua Tang, Zhi Fang, and Suo Yang. Practical formula for the estimation of cable tension in frequency method considering the effects of boundary conditions. *Hunan Daxue Xuebao/Journal of Hunan University Natural Sciences*, 2012.

[26] M Géradin and D Rixen. *Mechanical Vibrations: Theory and Application to Structural Dynamics*. Wiley, 1997.

[27] P. M. Morse, K. U. Ingard, and F. B. Stumpf. Theoretical Acoustics. *American Journal of Physics*, 1970.

[28] Francesco Foti, Margaux Geuzaine, and Vincent Denoël. On the identification of the axial force and bending stiffness of stay cables anchored to flexible supports. *Applied Mathematical Modelling*, 2020.

[29] Suzhen Li, Edwin Reynders, Kristof Maes, and Guido De Roeck. Vibration-based estimation of axial force for a beam member with uncertain boundary conditions. *Journal of Sound and Vibration*, 332(4):795–806, 2013.

[30] Giovanni Rebecchi, Nerio Tullini, and Ferdinando Laudiero. Estimate of the axial force in slender beams with unknown boundary conditions using one flexural mode shape. *Journal of Sound and Vibration*, 332(18):4122–4135, 2013.

[31] Chien Chou Chen, Wen Hwa Wu, Shin Yi Chen, and Gwolong Lai. A novel tension estimation approach for elastic cables by elimination of complex boundary condition effects employing mode shape functions. *Engineering Structures*, 166(March):152–166, 2018.

[32] Songhan Zhang, Ruili Shen, Yuan Wang, Guido De Roeck, and Geert Lombaert. A two-step methodology for cable force identification. *Journal of Sound and Vibration*, 472:115201, 2020.

[33] S. P. Timoshenko, J. M. Gere, and W. Prager. Theory of Elastic Stability, Second Edition. *Journal of Applied Mechanics*, 1962.

[34] S. Natsiavas. Mode Localization and Frequency Veering in a Non-Conservative Mechanical System With Dissimilar Components. *Journal of Sound Vibration*, 165(1):137–147, July 1993.

[35] Vincenzo Gattulli and Marco Lepidi. Localization and veering in the dynamics of cable-stayed bridges. *Comput. Struct.*, 85(21-22):1661–1678, November 2007.

[36] F.T.K. Au, Y.S. Cheng, Y.K. Cheung, and D.Y. Zheng. On the determination of natural frequencies and mode shapes of cable-stayed bridges. *Applied Mathematical Modelling*, 25(12):1099–1115, 2001.

[37] Delong Zuo Ming-Yi Liu and Nicholas P. Jones. Analytical and numerical study of deck-stay interaction in a cable-stayed bridge in the context of field observations. *Journal of Engineering Mechanics*, 139(11):1636–1652, 2013.

[38] Ahmed M. Abdel-Ghaffar and Magdi A. Khalifa. Importance of cable vibration in dynamics of cable-stayed bridges. *Journal of Engineering Mechanics*, 117(11):2571–2589, 1991.

[39] E. Caetano, A. Cunha, and C. A. Taylor. Investigation of dynamic cable-deck interaction in a physical model of a cable-stayed bridge. part i: modal analysis. *Earthquake Engineering & Structural Dynamics*, 29(4):481–498, 2000.

[40] Carlo Resta Anna De Falco and Giacomo Sevieri. Sensitivity analysis of frequency-based tie-rod axial load evaluation methods. *Engineering Structures*, 229:111568, 2021.

[41] K. Maes, J. Peeters, E. Reynders, G. Lombaert, and G. De Roeck. Identification of axial forces in beam members by local vibration measurements. *Journal of Sound and Vibration*, 332(21):5417–5432, 2013.

[42] Hiroshi Zui, Tohru Shinke, and Yoshio Namita. Practical formulas for estimation of cable tension by vibration method. *Journal of Structural Engineering*, 122(6):651–656, 1996.

[43] E.J. Hinch. *Perturbation Methods*. Cambridge University Press, Cambridge, 1995.

[44] Vincent Denoël and Thomas Canor. Patching asymptotics solution of a cable with a small bending stiffness. *Journal of Structural Engineering (United States)*, 2013.

[45] V. Denoël and E. Detournay. Multiple scales solution for a beam with a small bending stiffness. *Journal of Engineering Mechanics*, 136(1):69–77, 2010.

[46] Armin B. Mehrabi and Habib Tabatabai. Unified finite difference formulation for free vibration of cables. *Journal of Structural Engineering*, 124(11):1313–1322, 1998.

[47] M. Amabili, S. Carra, L. Collini, R. Garziera, and A. Panno. Estimation of tensile force in tie-rods using a frequency-based identification method. *Journal of Sound and Vibration*, 329(11):2057–2067, 2010.

[48] Joseph Penzien and Ray W. Clough. Dynamics of structures. *Earthquake Engineering Handbook*, pages 3–1–3–40, 2002.

[49] Z. Y. Shi, S. S. Law, and L. M. Zhang. Structural damage detection from modal strain energy change. *Journal of Engineering Mechanics*, 126(12):1216–1223, 2000.

[50] Faisal Shabbir, Muhammad Imran Khan, Naveed Ahmad, Muhammad Fiaz Tahir, Naeem Ejaz, and Jawad Hussain. Structural damage detection with different objective functions in noisy conditions using an evolutionary algorithm. *Applied Sciences*, 7(12), 2017.

[51] Ricardo Perera and Ronald Torres. Structural damage detection via modal data with genetic algorithms. *Journal of Structural Engineering*, 132(9):1491–1501, 2006.

[52] Rongrong Hou, Yong Xia, and Xiaoqing Zhou. Structural damage detection based on l1 regularization using natural frequencies and mode shapes. *Structural Control and Health Monitoring*, 25(3):e2107, 2018. e2107 STC-17-0060.R1.

[53] Jiawei Xiang, Ming Liang, and Yumin He. Experimental investigation of frequency-based multi-damage detection for beams using support vector regression. *Engineering Fracture Mechanics*, 131:257–268, 2014.

[54] Siu-Kui Au. *Operational Modal Analysis*. Springer Singapore, 01 2017.

[55] Gilles Tondreau and Arnaud Deraemaeker. Numerical and experimental analysis of uncertainty on modal parameters estimated with the stochastic subspace method. *Journal of Sound and Vibration*, 333(18):4376–4401, 2014.

[56] Rune Brincker. Some elements of operational modal analysis. *Shock and Vibration*, 2014, 2014.

[57] Rainer Storn and Kenneth Price. Differential Evolution - A Simple and Efficient Heuristic for Global Optimization over Continuous Spaces. *Journal of Global Optimization*, 1997.

[58] Swagatam Das, Ajith Abraham, Uday K. Chakraborty, and Amit Konar. Differential evolution using a neighborhood-based mutation operator. *IEEE Transactions on Evolutionary Computation*, 2009.

[59] Swagatam Das, Sankha Subhra Mullick, and P. N. Suganthan. Recent advances in differential evolution-An updated survey. *Swarm and Evolutionary Computation*, 2016.

[60] Karin Zielinski and Rainer Laur. Stopping criteria for differential evolution in constrained single-objective optimization. *Studies in Computational Intelligence*, 2008.

CRediT Author Statement

Identifiability of flexural boundary conditions in cables using natural frequencies and mode shapes for monitoring applications

Margaux Geuzaine: Conceptualization, Methodology, Software, Validation, Investigation, Writing (Original Draft), Visualization, Supervision

Francesco Foti: Conceptualization, Methodology, Supervision

Vincent Denoël: Conceptualization, Methodology, Writing (Review & editing), Project administration, Funding acquisition.

Declaration of interests

☒ The authors declare that they have no known competing financial interests or personal relationships that could have appeared to influence the work reported in this paper.

☐The authors declare the following financial interests/personal relationships which may be considered as potential competing interests: